Engineering Transactions, **67**(2): 167–184, 2019, doi: 10.24423/EngTrans.964.20190426
Polish Academy of Sciences • Institute of Fundamental Technological Research (IPPT PAN)
Université de Lorraine • Poznan University of Technology

The Effect of Strength Differential on Material Effort and Lifetime of Steam Turbine Rotors Under Thermo-Mechanical Load

Mariusz BANASZKIEWICZ[1)*], Waldemar DUDDA[2)], Janusz BADUR[1)]

[1)] *The Szewalski Institute of Fluid-Flow Machinery Polish Academy of Sciences*
Energy Conversion Department
Fiszera 14, 80-231 Gdańsk, Poland
e-mail: janusz.badur@imp.gda.pl
*Corresponding Author e-mail: mbanaszkiewicz@imp.gda.pl

[2)] *University of Warmia and Mazury, Faculty of Technical Sciences*
Oczapowskiego 11, 10-719 Olsztyn, Poland
e-mail: dudda@uwm.edu.pl

The paper presents the results of experimental tests and numerical simulations related with the strength differential effect. Tensile and compression tests on 2CrMoV low-alloy steel are performed to evaluate the magnitude of the yield stress difference in tension and compression. The strength differential parameter is then used in the formula for equivalent stress proposed by Burzyński. The material effort calculated using Burzyński and Huber-Mises-Hencky hypotheses was compared for different start-stop cycles. Analytical notch stress-strain correction rules by Neuber and Glinka-Molski were applied to compute elastic-plastic strain amplitudes in rotor circumferential grooves. It was finally shown that the strength differential effect has significant influence on the predicted fatigue life under thermo-mechanical loading.

Key words: strength differential; equivalent stress; steam turbine; rotor lifetime.

1. Introduction

A bulk of mechanical integrity analyses of machinery components employ the classical Huber-Mises-Hencky plasticity theory to define the equivalent stress and describe the plastic response of materials [1]. This theory assumes that the mean stress has no effect on plastic flow and the material is incompressible in the plastic regime. The classical definition of equivalent stress based on the second invariant of the deviatoric stress tensor J_2 neglects the strength differential effect, i.e. the difference of yield stresses in tension and compression, which was experimentally found in many materials [2]. For materials exhibiting this effect, a better match

of theoretical predictions with experimental stress-strain curves was found when the Burzyński yield condition was applied. According to the Burzyński hypothesis, the measure of material effort defining the limit of elastic range is a sum of the density of distortion elastic energy and a part of density of dilation elastic energy [3, 4]. The first contribution is related to the Huber-Mises-Hencky (HMH) equivalent stress, while the second part is a mean stress dependent. An extension of the Burzyński hypothesis accounting for the third invariant of stress tensor was proposed in [5, 6]. In this formulation the contribution of the density of elastic energy of distortion in material effort is controlled by the Lode angle. The recent application of the Burzyński-Drucker-Prager yield function with different friction angles to large strain thermoplasticity is presented in [7].

Vadillo *et al.* [1] simulated tensile tests on notched specimens of the 2024 T3 aluminium alloys as well as tests on the thin-walled tubes of Inconel 718 subjected to torsion after tension and compression. The comparison of numerical predictions with the experimental results revealed better correlation with experimental data of the plasticity theory with the Burzyński yield condition than that based on the Huber-Mises-Hencky criterion. The authors generally concluded that the plasticity theory with the paraboloid yield condition can adequately describe the strength differential (SD) effect present also in other materials, as e.g. high strength alloys or polymers.

Banaś and Badur [8] analysed a turbine guide vane from helicopter engine made of Inconel 718 assuming constant strength differential parameter $k = 1.1$ (at room temperature) due to the lack of experimental data. Conjugate heat transfer analysis was performed to obtain the temperature field, and elastoplastic stress analysis was then carried out using boundary conditions obtained from the CFD (computational fluid dynamics) analysis. The maximum difference in equivalent stress of 10% was found between the two failure criteria, i.e. Burzyński and Huber-Mises-Hencky.

The aim of the present work is to investigate the existence of strength differential effect in 2CrMoV creep-resistant steel used for high-temperature steam turbine rotors. Mechanical tests at room temperature were carried out and the obtained strength differential parameter was further used in stress analyses. Analytical notch stress-strain correction methods were applied to obtain strain amplitudes in elastic-plastic conditions. Finally, the low-cycle fatigue lives predicted using different definitions of equivalent stress and different strain correction methods were compared.

2. Burzyński yield condition

Burzyński [3, 4] proposed an energy-based hypothesis of material effort for materials which reveal difference in the failure strength in tension and compres-

sion. The hypothesis assumes the measure of material effort as a sum of the density of elastic energy of distortion and a part of density of elastic energy of the volume change. This statement is mathematically expressed as [9, 10]:

$$\Phi_f + \eta\,\Phi_v = K, \tag{2.1}$$

where the parameter $\eta = \omega + \frac{\delta}{3\sigma_m}$ depends on the material parameters ω and δ representing the contribution of the density of elastic energy of the volume change depending on the mean stress $\sigma_m = \frac{1}{3}\sigma_{ii}$. The constant K corresponds to the value of elastic energy density in a limit state.

Defining the density of elastic energy of distortion as [2]

$$\Phi_f = \frac{1}{12G}\left[(\sigma_1-\sigma_2)^2 + (\sigma_2-\sigma_3)^2 + (\sigma_3-\sigma_1)^2\right] \tag{2.2}$$

and the density of elastic energy of the volume change as [2]

$$\Phi_v = \frac{1-2\nu}{12G(1+\nu)}(\sigma_1+\sigma_2+\sigma_3)^2. \tag{2.3}$$

Introducing the above definitions of energy densities into Eq. (2.1) yields

$$\frac{2}{3}\sigma_e^2 + \frac{3(1-2\widetilde{\nu})}{(1+\widetilde{\nu})}\omega\sigma_m^2 + \frac{1-2\widetilde{\nu}}{(1+\widetilde{\nu})}\delta\sigma_m = 4GK, \tag{2.4}$$

where $\widetilde{\nu} = \frac{\sigma_y^C\sigma_y^T}{2\left(\sigma_y^S\right)^2} - 1$, $K = \frac{2\sigma_y^C\sigma_y^T}{12G(1+\widetilde{\nu})}$, and σ_e is the Huber-Mises-Hencky equivalent stress. The triplet (ω, δ, K) is substituted by Burzyński by the triplet (σ_y^C, σ_y^T, σ_y^S) which is obtained from commonly performed strength tests: σ_y^C – yield stress in compression, σ_y^T – yield stress in tension and σ_y^S – yield stress in torsion. This leads to the following form of the yield condition [1]:

$$\frac{\sigma_y^C\sigma_y^T}{3\left(\sigma_y^S\right)^2}\sigma_e^2 + \left(9 - \frac{3\sigma_y^C\sigma_y^T}{\left(\sigma_y^S\right)^2}\right)\sigma_m^2 + 3\left(\sigma_y^C - \sigma_y^T\right)\sigma_m - \sigma_y^C\sigma_y^T = 0. \tag{2.5}$$

This equation describes the plasticity surface in the space of principal stresses and its shape depends on the relation between the yields stresses (σ_y^C, σ_y^T, σ_y^S). For $3\sigma_y^S > \sigma_y^C\sigma_y^T$ the plasticity surface has the shape of an ellipsoid, for $3\sigma_y^S < \sigma_y^C\sigma_y^T$ the surface is a hyperboloid, while in case $3\sigma_y^S = \sigma_y^C\sigma_y^T$ the surface has the shape of a paraboloid of revolution [11, 12]. In this particular case Eq. (2.5) simplifies to the form:

$$\sigma_e^2 + 3\left(\sigma_y^C - \sigma_y^T\right)\sigma_m - \sigma_y^C\sigma_y^T = 0. \tag{2.6}$$

Equation (2.6) represents a parabola in the plane (σ_e, σ_m). After solving it with respect to σ_y^T and extracting a positive root, the final form of Burzyński yield condition is obtained [8]:

$$F(\sigma_e, \sigma_m) = \frac{1}{2k}\left[3(k-1)\sigma_m + \sqrt{9(k-1)^2\sigma_m^2 + 4k\sigma_e^2}\right] - \sigma_y^T = 0. \tag{2.7}$$

The Burzyński equivalent stress has thus the following form [8]

$$\sigma_B = \frac{1}{2k}\left[3(k-1)\sigma_m + \sqrt{9(k-1)^2\sigma_m^2 + 4k\sigma_e^2}\right]. \tag{2.8}$$

In the particular case when $k = 1$ (no strength differential effect present), the Burzyński equivalent stress is equal to the classical Huber-Mises-Hencky stress.

3. Laboratory tests of 2CrMoV steel

High-temperature rotors operating at temperature below 540°C are usually made of 2CrMoV creep-resistant steel of the bainitic microstructure. Test data showing the magnitude of strength differential in tension and compression are not available, so to evaluate this quantity laboratory tests on material samples were required. Round specimens made from this steel were used in uniaxial tensile and compression tests conducted at room temperature. Tensile tests were performed on 6 specimens having gauge length $L_0 = 35$ mm and diameter $d_0 = 7$ mm (Fig. 1a). For compression tests also 6 specimens of gauge height $h_0 = 18$ mm and diameter $d_0 = 12$ mm were prepared (Fig. 1b). The main dimensions of tensile and compression specimens are given in Table 1 and 2, respectively.

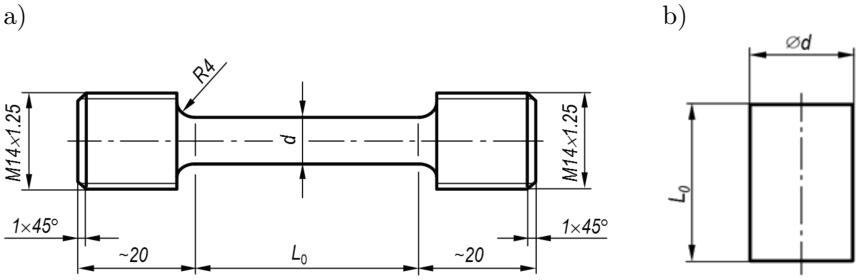

Fig. 1. Tensile (a) and compression (b) test specimens.

Table 1. Main dimensions of tensile specimens.

Specimen No	T1	T2	T3	T4	T5	T6
L_0 [mm]	35.00	35.00	35.00	35.00	35.00	35.00
d [mm]	7.00	7.01	7.00	7.01	6.99	6.99

Table 2. Main dimensions of compression specimens.

Specimen No	C1	C2	C3	C4	C5	C6
d [mm]	12.01	12.05	12.05	12.06	12.07	12.02
L_0 [mm]	18.05	18.05	18.05	18.05	18.05	18.05

Figure 2a presents pictures of tensile specimens after fracture together with detailed views of the fracture surfaces. All six specimens fractured at approximately the same section and the fracture surfaces had similar appearance typical for a ductile fracture with cup and cone features. Figure 2b shows the compression specimens at the end of the test with characteristic barreling typical for specimens with $L/d < 2$.

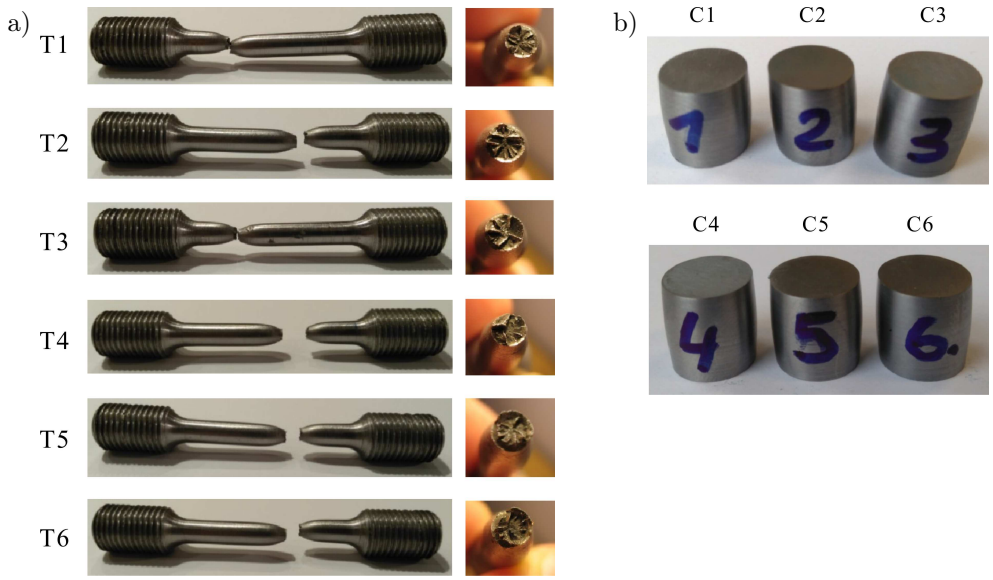

FIG. 2. Tensile (a) and compression (b) test specimens after failure.

As a result of testing, six stress-strain curves for tension and compression were obtained and they are shown in Fig. 3. The shape of all curves is similar and shows no irregularities which could indicate the presence of material flaws or imperfections. Little scatter of test data was observed in the plastic parts of the stress-strain curves. The yield stresses in tension and compression are given in Table 3 together with their scatter and mean values. The scatter of the yield stresses was approximately 20 MPa which is less than 3% of the mean values. As it is seen from the table, the average yield stress in compression is visibly higher than that in tension and their difference is around 10% which is 3 times higher than the scatter of yield stresses.

a)

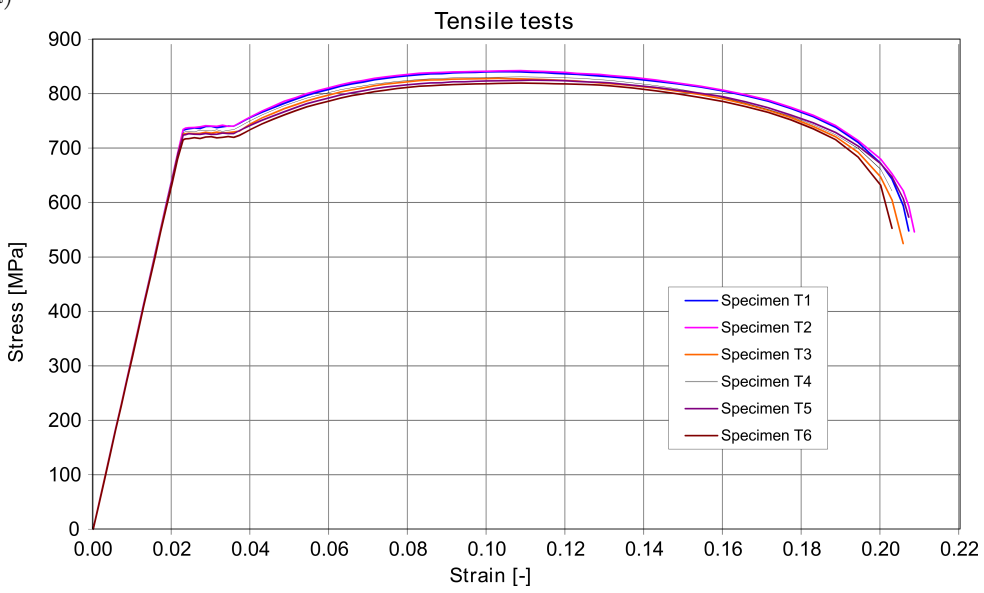

b)

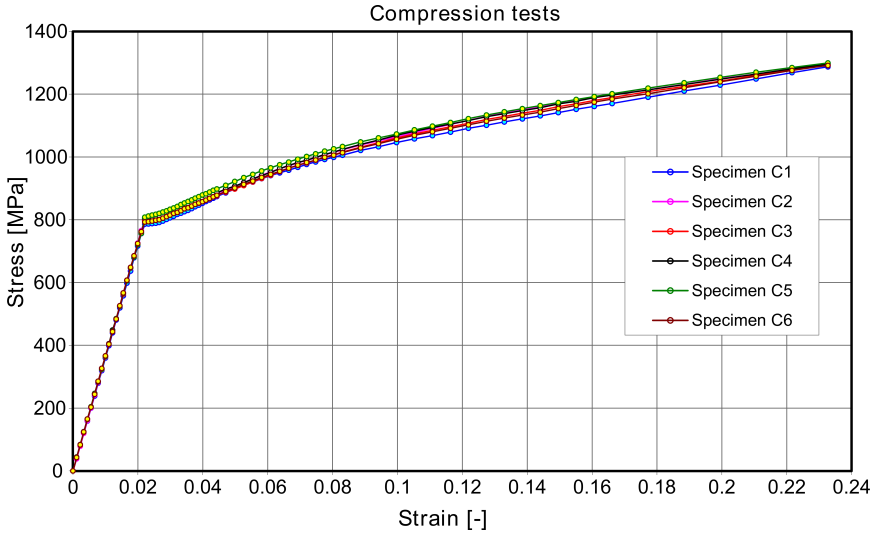

FIG. 3. Stress-strain curves for 6 tensile (a) and compression (b) specimens at 20°C.

Table 3. Yield stresses in tension and compression.

Specimen No	1	2	3	4	5	6	Scatter	Mean value
Tension [MPa]	732.8	734.3	725.8	728.1	723.9	715.3	19.0	726.7
Compression [MPa]	785.8	801.7	797.7	804.9	808.2	792.5	22.4	798.5

Based on the individual stress-strain curves, average curves at tension and compression were derived and are presented in Fig. 4 which clearly shows significant differences between the two curves in plastic conditions. The average yield stress at tension was $\sigma_y^T = 727$ MPa, while at compression reached $\sigma_y^C = 798$ MPa, which results in their ratio of $k = 1.1$. This value of strength differential was adopted in further numerical investigations. Recent results of laboratory tests carried out at high temperatures show that the value of k is almost constant and close to 1.1 which confirms the validity of results and conclusions drawn in this work.

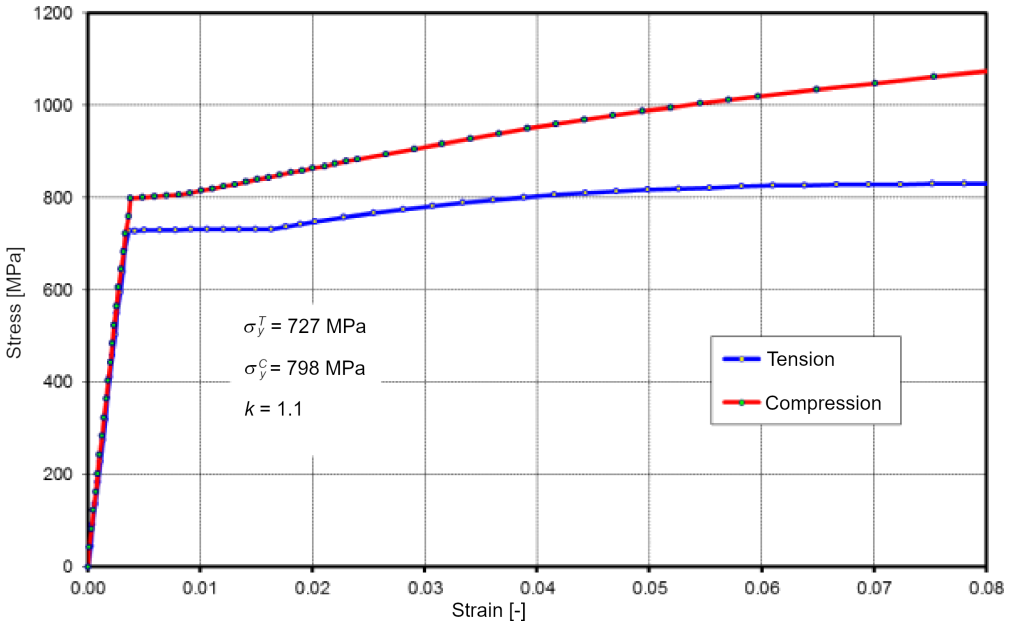

FIG. 4. Average stress-strain curves of 2CrMoV steel at tension and compression.

The Burzyński yield stress curve according to Eq. (2.7) is compared in Fig. 5 with the Huber-Mises-Hencky yield line for the analysed 2CrMoV steel. Both yield stresses have the same values equal to the yield stress in tension for the mean stress $\sigma_m = \frac{1}{3}\sigma_y^T = 242.2$ MPa. For higher mean stresses, the Burzyński yield stress becomes lower than the Huber-Mises-Hencky stress, and for lower mean stresses it is higher. For zero mean stress, the Burzyński yield stress is equal to the geometric average of the yield stress in tension and compression. For the mean stress $\sigma_m = -\frac{1}{3}\sigma_y^C$, the Burzyński yield stress is equal to the yield stress in compression. The major observation is that in compression and in a significant part of tension, the strength differential has a positive effect on material effort

expressed by increased yield stress according to Burzyński comparing with the Huber-Mises-Hencky yield stress.

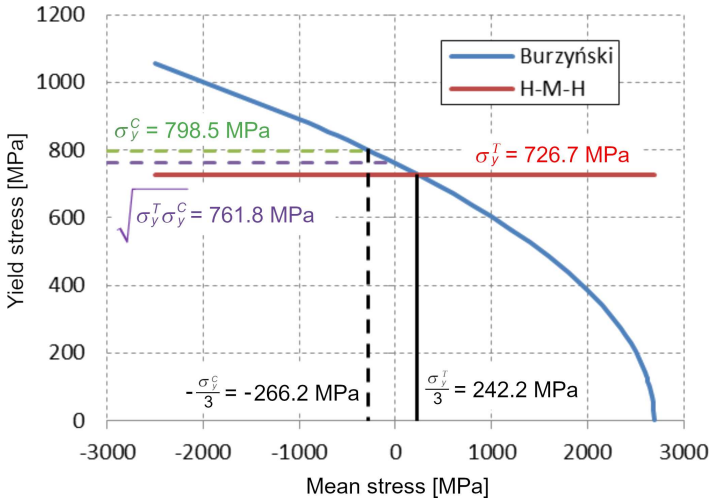

FIG. 5. Burzyński yield stress curve at 20°C.

4. Notch stress-strain correction methods

Thermoelastic notch stresses in the areas of fatigue cracking exceed the material yield stress and consideration of elastic-plastic material response is crucial for a proper estimation of fatigue life. Cyclic plasticity models are best suited for this purpose, but for preliminary studies analytical stress-strain correction methods can be successfully applied. The most commonly used methods for elastic-plastic stress-strain correction basing on the elastic solution are Neuber's rule [13] and the Glinka-Molski equivalent strain energy density method [14]. In case of multi-axial state of stress and strain, the extended Neuber rule is used [15]:

$$\sigma_e \varepsilon_e = \sigma_e^{el} \varepsilon_e^{el}, \tag{4.1}$$

where σ_e – equivalent stress, ε_e – equivalent strain, σ_e^{el} – equivalent stress obtained from elastic solution, ε_e^{el} – equivalent strain obtained from elastic solution. The equivalent strains are defined using mechanical strain components.

Similarly, the Glinka-Molski method was extended for multi-axial state of stress using the definition of strain energy density [16]:

$$\frac{1}{2}\sigma_e^{el}\varepsilon_e^{el} = \int_0^{\varepsilon_e} \sigma_e \, \mathrm{d}\varepsilon_e. \tag{4.2}$$

Graphical interpretation of both methods for elastic-linear strain hardening material is given in Figs 6 and 7. The Neuber rule (Fig. 6) assumes the equality of the total strain energy density at the notch tip in elastic (grey area under $\sigma_e^{el} - A - \varepsilon_e^{el}$ curve) and elastic-plastic states (shaded area under $\sigma_e - B - \varepsilon_e$ curve). The total strain energy density is defined as the sum of the strain energy density and the complementary strain energy density.

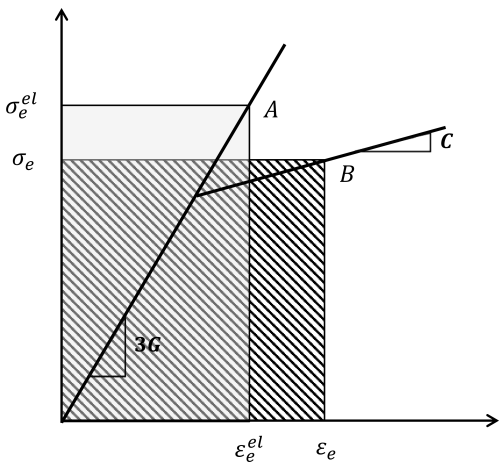

FIG. 6. Graphical interpretation of the Neuber rule.

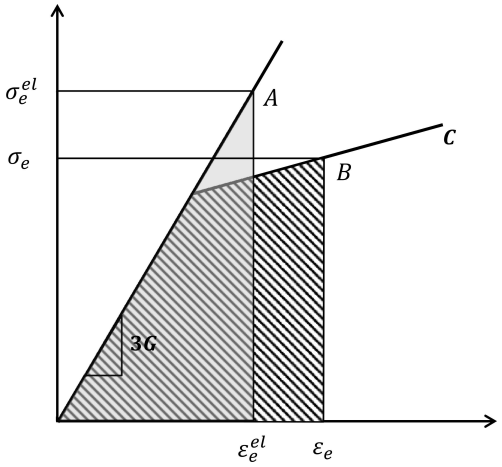

Fig. 7. Graphical interpretation of the Glinka-Molski method.

The Glinka-Molski method (Fig. 7) assumes the equality between the strain energy density at the notch tip of a linear elastic body (grey area under elastic curve under $\sigma_e^{el} - \varepsilon_e^{el}$) and the strain energy density at the notch tip of a geometrically identical elastic-plastic body (grey area under elastic-plastic stress-strain curve $\sigma_e - \varepsilon_e$) subjected to the same load.

The formulations of Neuber's rule and Glinka-Molski's method given by Eqs (4.1) and (4.2) are based on the definitions of equivalent stress and strain according to Huber-Mises-Hencky hypothesis, and neglect the contribution of dilatation energy representing the influence of mean stress [17]. In case when the Burzyński equivalent stress definition is applied, which includes the effect of mean stress, the contribution of dilatation energy is implicitly modelled by the equivalent stress, and the use of formulations based on equivalent stress and strain (Eqs (4.1) and (4.2)) is better justified than for the case of the Huber-Mises-Hencky equivalent stress.

Recalling the definition of the equivalent stress σ_e expressed by the deviatoric stress components s_{ij} [18]:

$$\sigma_e = \sqrt{\frac{3}{2} s_{ij} s_{ij}}, \tag{4.3}$$

and the equivalent strain ε_e is defined by the deviatoric strain components e_{ij} with energy conjugate strain definition:

$$\varepsilon_e = \sqrt{\frac{2}{3} e_{ij} e_{ij}}. \tag{4.4}$$

For proportional loading conditions and multiaxial state of stress, the equivalent strain can be expressed as a sum of equivalent elastic strain ε_e^{el} and equivalent plastic strain ε_e^{pl} [19]

$$\varepsilon_e = \varepsilon_e^{el} + \varepsilon_e^{pl}. \tag{4.5}$$

The equivalent elastic strain is defined as

$$\varepsilon_e^{el} = \frac{1}{3G} \sigma_e, \tag{4.6}$$

where G is shear modulus, and the equivalent plastic strain in a linear kinematic model can be expressed as

$$\varepsilon_e^{pl} = \frac{1}{C} (\sigma_e - \sigma_y), \tag{4.7}$$

where σ_y is material proof stress, and C is a kinematic hardening parameter.

For cyclic stress-strain analysis, Eqs (4.1) and (4.2) are re-written for the corresponding stress and strain amplitudes [20, 21]

$$\sigma_{e,a} \varepsilon_{e,a} = \sigma_{e,a}^{el} \varepsilon_{e,a}^{el}, \tag{4.8}$$

$$\frac{1}{2} \sigma_{e,a}^{el} \varepsilon_{e,a}^{el} = \int_0^{\varepsilon_{e,a}} \sigma_{e,a} \, \mathrm{d}\varepsilon_{e,a}. \tag{4.9}$$

The above two equations were used to determine elasto-plastic strain amplitudes at the notch tip based on the stress and strain histories obtained from elastic material response.

Equations (4.8) and (4.9) can be transformed to quadratic equations using the strain definitions (4.5)–(4.7) under the assumption of linearly kinematic hardening material and proportional loading conditions [22]:

- for the Neuber rule:

$$C \varepsilon_{e,a}^2 + \left(\sigma_y - \frac{1}{3G} C \sigma_y \right) \varepsilon_{e,a} - \frac{1}{3G} \left(\sigma_{e,a}^{el} \right)^2 = 0, \tag{4.10}$$

- for the Glinka-Molski method:

$$C\varepsilon_{e,a}^2 + \left(2\sigma_y - \frac{2}{3G}C\sigma_y\right)\varepsilon_{e,a} + \frac{1}{9G^2}\left[C(\sigma_y)^2 - 3G(\sigma_{e,a}^{el})^2 - 3G(\sigma_y)^2\right] = 0. \tag{4.11}$$

The above two equations can be solved analytically by means of the discriminant method to obtain the strain amplitudes in the elastic-plastic state $\varepsilon_{\mathrm{eq},a}$. The existence of analytical solutions for strain amplitude is very important from the perspective of practical application to fatigue life analysis. Analytical expression for the strain amplitude can be used in lifetime calculations when a large number of cycles is to be analysed or for online monitoring of fatigue damage. These two formula are employed in the next section in investigations of fatigue life of a steam turbine rotor.

5. Stress and lifetime analysis of a steam turbine rotor

The material effort of a steam turbine rotor subject to thermo-mechanical loading was investigated by performing transient finite element analysis using Abaqus program [23]. A linear elastic material model was adopted together with temperature-dependent material properties and nonlinear thermal boundary conditions varying in time and space. The material physical properties in thermal (conductivity, specific heat) and mechanical (Young modulus, thermal expansion coefficient, Poisson ratio) analysis were provided in a tabular form for temperature varying from 20°C to 550°C and used by the program as a piecewise linear function. The de-coupled thermo-elasticity problem was solved: temperature distribution in the rotor was obtained by solving the Fourier-Kirchhoff equation written in cylindrical co-ordinate system for the rotor axisymmetric geometry and based on the temperature field, stress and strain distributions were obtained in the second step. The rotor temperature and Huber-Mises-Hencky stress distributions during a cold start are shown in Fig. 8. The rotor temperature distribution (Fig. 8a) is highly non-uniform and exhibits radial and axial temperature gradients induced by axial gradients of steam temperature and heat transfer coefficient. The rotor thermomechanical stress field is generally more uniform (Fig. 8b) but very small areas of high stress concentration are found in the circumferential grooves acting as geometrical notches (shown for example as G1, G3 and G6). The grooves are located in the hottest region of the rotor and peak stresses occur at the bottom of the grooves (notch tip). At the notch tip the stress can exceed the material initial yield stress and significant plastic deformation can occur in a very tiny zone [24].

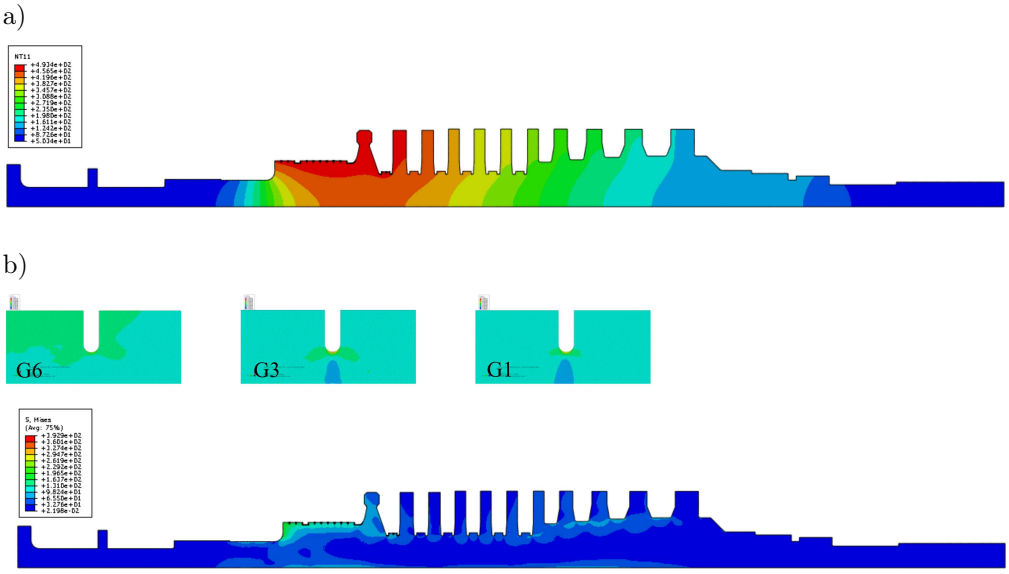

FIG. 8. Rotor temperature (a) and equivalent stress distribution (b) during a cold start.

Variations in time of the mean stress and the equivalent stresses evaluated at the circumferential U-groove G3 using both Burzyński and Huber-Mises-Hencky hypotheses are shown in Fig. 9. The Huber-Mises-Hencky and mean stress is taken directly from Abaqus analysis while the Burzyński equivalent stress is post-processed based on these two stresses using the formula (2.8). It presents stress variations for complete start-stop cycles, where the start-up phase is accompanied by rotor heating-up generating compressive stress at the surface, and the subsequent shutdown resulting in cooling-down and tensile surface stress. The Burzyński stress was calculated assuming constant temperature-independent yield stress ratio $k = 1.1$. For all three considered start-stop cycles, during heating the Huber-Mises-Hencky stress is visibly higher than that obtained with the Burzyński hypothesis. In this phase, the mean stress is negative and lower than $1/3\sigma_e$, but when it exceeds this limit, the Burzyński stress becomes slightly higher. The operation phase when the mean stresses are negative corresponds to the rotor heating-up, while the positive mean stresses are present in steady-state and during cooling-down phase. Thus, high compressive stress states reduce the material effort and due to the strength differential effect allow for higher HMH stresses during heating-up without adversely affecting the rotor material effort. This is of high practical importance as the rotor heating-up takes place during turbine start-up and more accurate determination of the equivalent stress can allow for better utilization of material strength and results in a reduction of the start-up time.

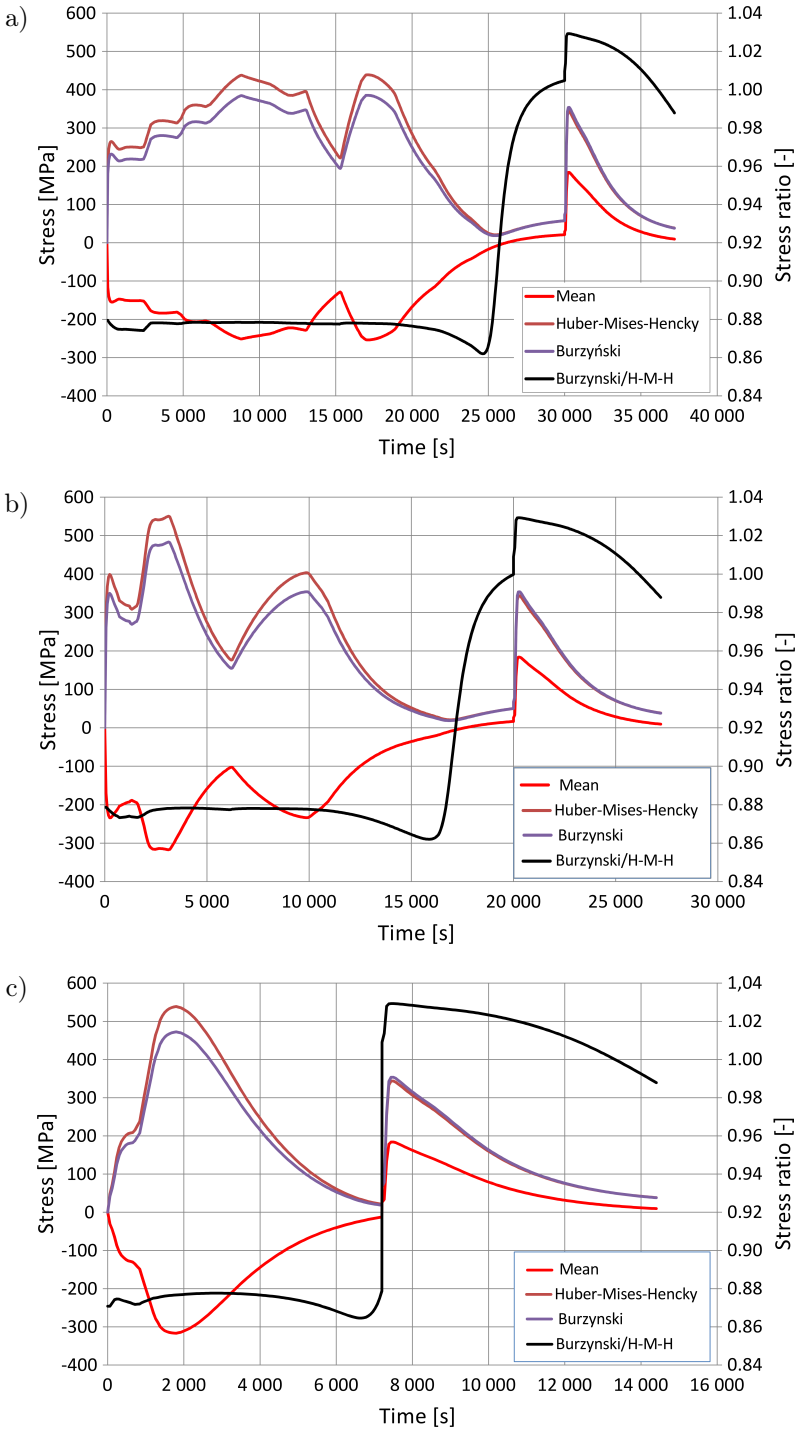

FIG. 9. Variations of stresses and stress ratio for the cold (a), warm (b) and hot (c) start cycle.

It is also observed that the stress ratio at the groove is relatively constant during rotor heating-up and for all three starts varies within 0.86–0.88. A considerable increase of the stress ratio takes place when the state of stress changes from compression into tension causing it to raise above 1 at the instant of peak tensile stress during shutdown.

The Neuber rule and the Glinka-Molski method described in Sec. 4 were adopted for thermo-elasto-plastic strain analysis. The equivalent stress in elastic state was evaluated using Burzyński and Huber-Mises-Hencky hypotheses and then used to obtain the strain amplitude in the elastic-plastic condition by solving Eqs (4.10) and (4.11). The temperature-dependent yield stress $\sigma_y(T)$ was used in calculations to take into account high variations of temperature occurring during start-ups. The temperature-dependent yield stress was adopted from the available material card for this steel and taking into account the cyclic softening factor equal 0.8. The minimum value of 0.2% proof stress (i.e. stress to produce 0.2% plastic strain) was approximated by a 6th order polynomial of temperature and used in Eqs (4.10) and (4.11) to obtain analytically strain amplitudes. The results are presented in Fig. 10 showing the relation between strain amplitudes computed using the two analysed equivalent stress definitions applied to different start-up cycles. The strain amplitudes obtained using Burzyński hypotheses are in all cases lower than those calculated on the basis of the Huber-Mises-Hencky yield condition (all points lie below the 1:1 proportionality line). It was also found that the Glinka-Molski method predicts lower strain amplitudes than the Neuber rule which is in agreement with the previous studies [25]. The minimum strain amplitude ratio of 0.9 (strain amplitude from Burzyński hypothesis divided by the corresponding amplitudes from Huber-Mises-Hencky hypotheses) was obtained for the hot start (HS) using the Neuber rule, while the maximum ratio was obtained for the cold start (CS) when the Glinka-Molski strain correction method was applied.

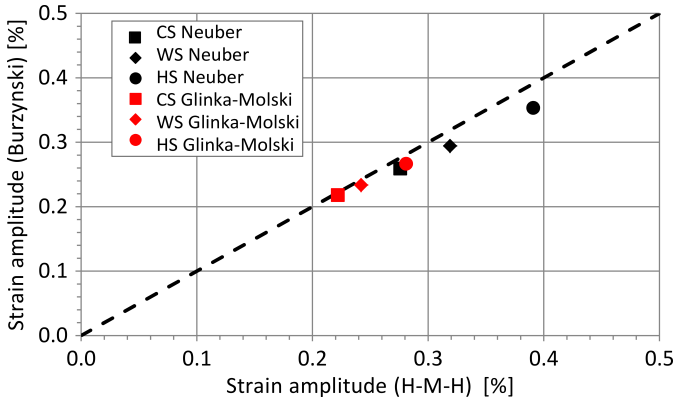

FIG. 10. Strain amplidues obtained for different cycles using Neuber and Glinka-Molski method.

Extreme values of the stress ratio for each transient event are summarized in Table 4. Both the extreme values in the event and the values at stress maximum are similar for all start-up types. For the shutdown phase the extreme values are less variable and are approximately 1.

Table 4. Equivalent stress ratios for different transient events.

Event type	Minimum in event	Maximum in event	At maximum stress
Cold start	0.862	1.005	0.878
Warm start	0.862	1.009	0.878
Hot start	0.865	1.009	0.877
Shutdown	0.998	1.029	1.029

The number of cycles to crack initiation was evaluated by using the strain-life method and the low-cycle fatigue data with hold time accounting for the creep damage due to secondary loading [17]. The results of fatigue life predicted using the analysed equivalent stress definitions and stress-strain correction methods are compared in Fig. 11. In case of the number of cycles, the values obtained using Burzyński hypotheses are above those calculated on the basis of the Huber-Mises-Hencky yield condition (all points lie above the 1:1 line). The maximum ratio of the number of cycles equal 2.11 was obtained for the hot start using the Neuber rule, while the minimum ratio of 1.07 was predicted for the cold start when the Glinka-Molski method was used. This is a considerable scatter of fatigue life, in particular for the hot start cycle where the lowest values of fatigue endurances were predicted. The results of investigations clearly show considerable differences in fatigue lives obtained using both methods and indicate the beneficial effect of

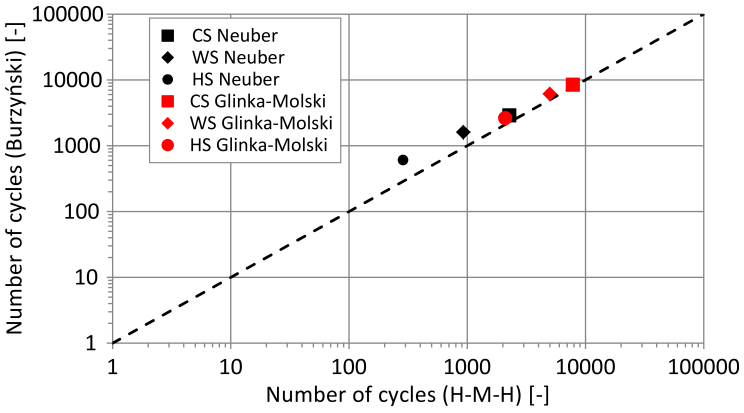

FIG. 11. Number of cycles to cracking obtained for different cycles using Neuber and Glinka-Molski method.

the mean stress preferring the use of Burzyński yield condition when significant compressive state of stress persists.

6. Summary

The existence of strength differential effect in 2CrMoV rotor steel was proved experimentally and its positive effect on the material effort was shown by numerical simulations of the rotor during transient operating conditions. The measured magnitude of the strength differential $k = 1.1$ results in the equivalent stress ratio reaching a minimum of 0.86 at the circumferential U-groove during the compressive phase of the cycle. Elastic-plastic strain amplitudes evaluated using analytical stress-strain correction methods were found to be lower when the strength differential effect was included in the yield condition as compared with the predictions of the classical J_2 plasticity theory. The minimum strain amplitude ratio of 0.9 obtained for the hot start-stop cycle resulted in a more than 2 times longer fatigue life. This demonstrates that the use of the Burzyński hypothesis allows for better utilization of material strength or fatigue life extension provided that the strength differential effect is experimentally confirmed. The high difference in fatigue lives obtained using both methods indicates the beneficial effect of the mean stress preferring the use of the Burzyński yield condition when significant compressive state of stress persists.

The results presented in this paper should be considered as an initial outcome of the investigations showing only a potential for improvement in the analyses of material effort and lifetime of steam turbine rotors. Continued material tests are on-going with the aim to investigate the variation of strength differential with temperature. The next steps of the research will be to carry out cyclic tension-compression tests in a range of temperatures and implement the Burzyński yield criterion in the finite element programme to describe more accurately the stress-strain state in elastic-plastic conditions.

References

1. Vadillo G., Fernandez-Saez J., Pęcherski R.B., *Some applications of Burzynski yield condition in metal plasticity*, Materials and Design, **32**: 628–635, 2011.
2. Frąś T., Kowalewski Z., Pęcherski R.B., Rusinek A., *Applications of Burzynski failure criteria – I. Isotropic materials with asymmetry of elastic range*, Engineering Transactions, **58**: 1–10, 2010.
3. Burzyński W., *About the effort hypotheses* [in German: *Über die Anstrengungshypothesen*], Schweiz Bauzeitung, **94**(21): 259–262, 1929 (reprinted in: Burzyński W., *Selected works*, Vol. I, PAN–PWN, Warszawa, pp. 259–262, 1982).
4. Burzyński W., *Theoretical foundations of the hypotheses of material effort*, Engineering Transactions, **56**(3): 269–305, 2008 (the recent edition of English translation of the paper

[in Polish: *Teoretyczne podstawy hipotez wytężenia*], Czasopismo Techniczne, **47**: 1–41, 1929).

5. Nowak M., Ostrowska-Maciejewska J., Pęcherski R.B., Szeptyński P., *Yield criterion accounting for the third invariant of stress tensor deviatore. Part I. Proposition of the yield criterion based on the concept of influence functions*, Engineering Transactions, **59**(4): 273–281, 2011.
6. Pęcherski R.B., Szeptyński P., Nowak M., *An extension of Burzynski hypothesis of material effort accounting for the third invariant of stress tensor*, Archives of Metallurgy and Materials, **56**(2): 503–508, 2011.
7. Mucha M., Wcisło B., Pamin J., Kowalczyk-Gajewska K., *Instabilities in membrane tension: Parametric study for large strain thermoplasticity*, Archives of Civil and Mechanical Engineering, **18**: 1055–1067, 2018.
8. Banaś K., Badur J., *Influence of strength differential effect on material effort of a turbine guide vane based on a thermoelastoplastic analysis*, Journal of Thermal Stresses, **40**: 1368–1385, 2017.
9. Frąś T., Pęcherski R.B., *Applications of the Burzynski hypothesis of material effort for isotropic solids*, Mechnaics and Control, **29**(2): 45–50, 2010.
10. Pęcherski R.B., *Burzynski yield condition vis-à-vis the related studies reported in the literature*, Engineering Transactions, **56**(4): 383–391, 2008.
11. Życzkowski M., *Discontinuous bifurcation in the case of the Burzyński-Torre yield conditions*, Acta Mechnica, **132**: 19–35, 1999.
12. Ganczarski A., Skrzypek J., *Mechanics of modern materials – models, anizotropy, limit surfaces, composite materials, dissipative processes* [in Polish], Cracow University of Technology, Kraków, 2013.
13. Neuber H., *Theory of stress concentration for shear-strained prismatical bodies with arbitrary non-linear stress-strain law*, ASME Journal of Applied Mechanics, **28**: 544–550, 1961.
14. Molski K., Glinka G., *A method of elastic-plastic stress and strain calculation at a notch root*, Material Science and Engineering, **50**: 93–100, 1981.
15. Hoffman M., Seeger T., *A generalized method for estimating multiaxial elastic-plastic notch stresses and strains – Part I and II*, ASME Journal of Engineering Materials and Technology, **107**: 250–260, 1985.
16. Moftakhar A., Buczyński A., Glinka G., *Calculation of elasto-plastic strains and stresses in notches under multiaxial loading*, International Journal of Fracture, **70**: 357–373, 1995.
17. Banaszkiewicz M., *The low-cycle fatigue life assessment method for online monitoring of steam turbine rotors*, International Journal of Fatigue, 113, 311–323, 2018.
18. Kleiber M., Kowalczyk P., *Introduction to non-linear thermo-mechanics of deformable bodies* [in Polish: *Wprowadzenie do nieliniowej termomechaniki ciał odkształcalnych*], IPPT, Warsaw, 2011.
19. Harkegard G., Mann T., *Neuber prediction of elastic-plastic strain concentration in notched tensile specimens under large-scale yielding*, Journal of Strain Analysis, **38**: 79–94, 2003.

20. Zeng Z., Fatemi A., *Elasto-plastic stress and strain behaviour at notch roots under monotonic and cyclic loadings*, Journal of Strain Analysis, **36**: 287–300, 2001.

21. Banaszkiewicz M., *Multilevel approach to lifetime assessment of steam turbines*, International Journal of Fatigue, **73**: 39–47, 2015.

22. Lemaitre J., Desmorat R., *Engineering damage mechanics*, Springer-Verlag, Berlin–Heidelberg, 2005.

23. *Abaqus 6.12 User's manual*, 2012.

24. Banaszkiewicz M., Dudda W., *Applicability of notch stress-strain correction methods to low-cycle fatigue life prediction of turbine rotors subjected to thermomechanical loads*, Acta Mechanica et Automatica, **12**(3): 179–185, 2018.

25. Banaszkiewicz M., *Numerical investigations of crack initiation in impulse steam turbine rotors subject to thermo-mechanical fatigue*, Applied Thermal Engineering, **138**: 761–773, 2018.

Received October 7, 2018; accepted version January 25, 2019.
